

Initial Developments of a Low Drag Variable Depth Acoustic Liner

Noah H. Schiller,¹ Michael G. Jones², Brian M. Howerton³, Douglas M. Nark⁴

NASA Langley Research Center, Hampton, VA, 23681, USA

The purpose of this study is to assess the acoustic performance and relative drag of a new type of variable depth liner containing pairs of resonators coupled together by shared inlet volumes just below the facesheet. This type of liner has the potential to achieve a targeted impedance with fewer openings in the facesheet, and therefore less drag, than previous designs. To better understand the limitations of the concept, three sets of samples were designed and tested in the NASA Langley normal incidence and grazing flow impedance tubes. Each set of samples consisted of a baseline variable depth liner with straight chambers, and a prototype liner with shared inlet volumes. Measurements conducted in both the normal incidence and grazing flow impedance tubes confirm that the prototype liner can achieve the same impedance as the baseline variable depth liner at discrete frequencies with 50% less open area. This results in a 75% reduction in the drag penalty relative to the baseline design. The proposed concept is not, however, able to achieve a flat, broadband impedance as effectively as the baseline liner. So, while the proposed concept is well suited for multitonal design metrics, tradeoffs must be made between liner drag and acoustic performance when broadband attenuation is required.

I. Nomenclature

a	empirical constant
c, ρ	ambient sound speed and density, respectively
C_D	discharge coefficient
d, t	facesheet hole diameter and thickness, respectively
f	frequency
F	objective function
j	unit imaginary number
k	acoustic wavenumber
M_{CL}	centerline Mach number
N_f, N_r	number of frequencies and resonators, respectively
r, R	equivalent chamber radius and ratio of reflected to incident energy, respectively
S	cross sectional area
W	frequency weighting parameter
α	absorption coefficient
β_{avg}	normalized spatially averaged admittance

¹ Senior Research Scientist, Structural Acoustics Branch, MS 463, AIAA Member.

² Senior Research Scientist, Structural Acoustics Branch, MS 463, AIAA Associate Fellow.

³ Research Scientist, Structural Acoustics Branch, MS 463, AIAA Senior Member.

⁴ Senior Research Scientist, Structural Acoustics Branch, MS 463, AIAA Associate Fellow.

δ	end correction
δ^*, ε	boundary layer displacement thickness and hole length end correction multiplier, respectively
λ_L, λ_{SW}	resistance factors for the liner and smooth wall sample, respectively
$\Delta\lambda_L$	relative liner drag
μ	dynamic viscosity of air
σ	open area ratio
$\theta_{lin}, \theta_{nonlin}, \theta_{gf}$	linear, nonlinear, and grazing flow components of the normalized resistance, respectively
χ_{fs}, χ_{rad}	normalized facesheet reactance and radiation reactance, respectively
ω	circular frequency
$\zeta_s, \zeta_{opt}, \zeta_{target}$	normalized smeared surface impedance, optimal impedance, and target impedance, respectively
ζ'_A	normalized total resonator impedance

II. Introduction

New technologies are needed to mitigate the environmental impact of aircraft operations and enable sustainable growth of the aviation sector. To focus the development of these technologies, NASA and the FAA have set aggressive goals for fuel consumption and noise. One technology currently employed to reduce noise from aircraft engines is the acoustic engine liner. Engine liners typically consist of a perforated facesheet over a honeycomb core. The core forms discrete chambers below the facesheet, which act as an array of acoustic resonators. The facesheet protects the core from the harsh environment in the engine, couples the external acoustic field to the resonators in the core, and contributes acoustic resistance needed to convert incident acoustic energy to heat. Perforated facesheets, however, have a higher drag than smooth surfaces. The additional drag, in turn, has a negative impact on the fuel consumption of the vehicle. In the past, the drag penalty associated with the liner was tolerated to meet community noise goals. However, new technologies that minimize the drag penalty without degrading the acoustic performance are needed to enable simultaneous reductions of fuel consumption and noise.

In 2016, Ref. [1] showed that liner drag can be reduced without sacrificing acoustic performance. Specifically, this was achieved by replacing the standard perforated facesheet, which typically has round holes, with a facesheet that has perpendicular slots (i.e., the long dimension of the slot is perpendicular to the flow). This discovery led to additional laboratory studies, analysis, and recently culminated in a flight test [2]. While successful, additional reductions of the drag penalty are still needed. An experimental study conducted by Ref. [3] identified a strong relationship between the liner drag and the open area ratio of the facesheet. As the open area is reduced, the drag decreases, approaching the drag of a smooth wall as the open area goes to zero. For conventional liners, however, the open area ratio cannot be reduced without sacrificing acoustic performance.

New designs continue to be developed to improve the acoustic performance of engine liners. While conventional liners, which consist of an array of nominally identical resonators, are effective for tonal noise, modern aircraft engines also have a significant broadband component. Therefore, broadband concepts, such as variable depth liners, are also being developed. As the name implies, variable depth liners contain chambers with different depths tuned for different frequencies [4, 5]. While this offers acoustic benefits, variable depth liners still require perforated facesheets and, therefore, have a similar drag penalty as conventional liners.

This paper describes the design and evaluation of a new type of variable depth acoustic liner that can be used to reduce the open area ratio of the facesheet, and therefore drag penalty, without sacrificing acoustic performance. The paper begins with a description of the variable depth liner concept. Acoustic models used to evaluate the concept and design prototype liner samples are detailed next. A description of the samples and tests is provided. Finally, results are presented comparing the acoustic performance and relative liner drag of the proposed concept to a more conventional variable depth design.

III. Variable Depth Concept

In many applications, the acoustic liner is designed to have a specific frequency dependent behavior that provides multitonal or broadband attenuation. One way to control frequency dependence is to vary the depth of neighboring resonators within the liner, as depicted in Fig. 1(a). Within this type of liner, individual resonators are most effective near resonance where the magnitude of the acoustic particle velocity at the facesheet is large. In contrast, at off-resonance frequencies, the particle velocity at the facesheet is relatively low. In fact, at antiresonance, the particle velocity is zero. Thus, the resonators could be replaced by a solid wall with no impact on the overall acoustic

performance at that frequency. As long as neighboring resonators are tuned for different frequencies, it could be possible to combine resonators within the core of the liner and achieve similar acoustic performance with fewer openings in the facesheet. This concept is depicted in Fig. 1(b) and Fig. 1(c), where individual chambers are coupled together by shared inlet volumes just below the facesheet. Reducing the number of openings in the facesheet would, in turn, reduce the relative liner drag, and could also reduce fabrication time and cost. The purpose of this study is to assess the acoustic performance and relative liner drag of the proposed variable depth liner concept. To limit the scope of the investigation, the paper compares the conventional variable depth (VD) design shown in Fig. 1(a) with the shared inlet volume (SIV) concept depicted in Fig. 1(c). The conclusions, however, are also applicable to similar concepts, such as Fig. 1(b).

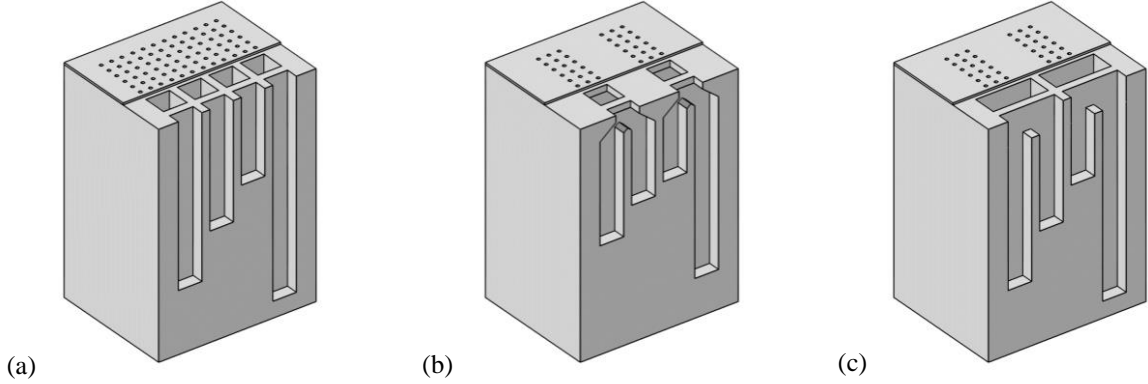


Fig. 1 Variable depth liner designs: (a) conventional variable depth (VD) design, (b) shared inlet volume (SIV) design, and (c) alternative SIV design with a simpler inlet geometry.

IV. Impedance Models

Two types of models are used in this study to predict the smeared surface impedance of the liner samples. An efficient semianalytical impedance model is used first to explore a relatively large design space. A more accurate, but also more computationally expensive, finite element model is then used to refine the design.

A. Semianalytical Impedance Model

Semianalytical models are derived for both types of liners using transmission line methods for the core coupled with lumped parameter models for the facesheet. The acoustic impedance of individual resonators within the sample are then combined to determine the smeared surface impedance of the sample.

1. Liner Core

Transmission line methods are well suited for predicting plane wave propagation in the core. The analysis begins at the back plate (i.e., the bottom surface of the liner farthest from the facesheet), and proceeds toward the facesheet, accounting for all impedance discontinuities within the core. For the variable depth sample depicted in Fig. 2(a), there are no impedance discontinuities within the core, and therefore, the specific acoustic input impedance of each chamber, just below the facesheet, can be found directly as

$$\zeta_i = -j \cot(kh_i) \quad (1)$$

where $j = \sqrt{-1}$, h_i is the depth of the chamber, $k = \omega/c$ is the acoustic wavenumber, ω is the circular frequency, and c is the speed of sound. Note that $e^{j\omega t}$ time convention is used here and throughout the rest of the paper. While losses within the chamber could be captured using a complex valued acoustic wavenumber [6], they are neglected in this study since the chambers are relatively large with a 0.4" by 0.4" cross section.

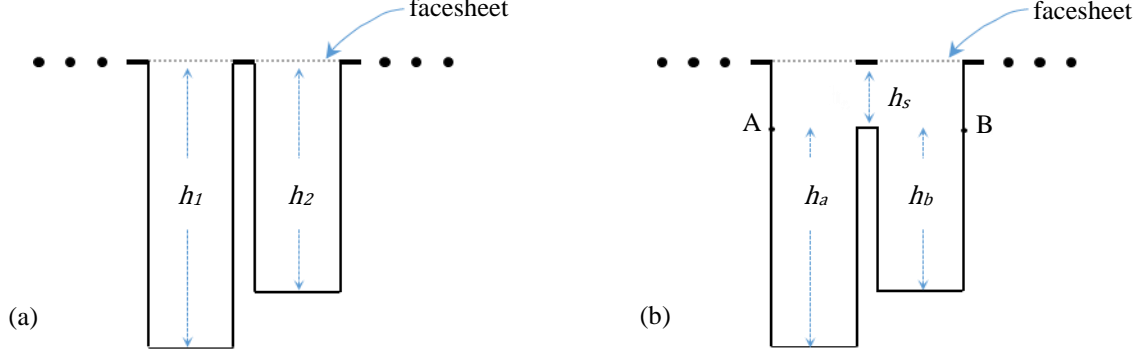


Fig. 2 Sketch of resonator geometry in the (a) VD sample, and (b) SIV sample.

The variable depth design with shared inlets, depicted in Fig. 2(b), has multiple impedance discontinuities within the core. More specifically, the design has independent chambers that are connected to a shared inlet volume just below the facesheet. To simplify the comparison between the two liner concepts, a thin strip of material is included on top of the shared inlet volume just below the facesheet. This reduces the cross sectional area of the shared inlet to match the inlet area of the conventional variable depth sample. The model is developed, once again, starting at the back plate. The effect of the lower chambers is captured with the $\cot(kh)$ function. At the intersection between the lower chambers and the shared inlet volume, the plane wave assumption breaks down due to the excitation of higher-order modes in the vicinity of the area change. This effect is captured with a lumped parameter correction similar to the end correction used by Ref. [7] for a centrally located orifice in a duct. In this case, however, the lower chambers are offset to one side of the shared volume, and therefore, a modified end correction is used [8]. The total impedance of chamber A at the intersection with the shared inlet volume is

$$\zeta'_A = j\cot(kh_a) + j\chi_{\text{rad}} \quad (2)$$

where $\chi_{\text{rad}} = k\delta$, $\delta = (2r)(8/(3\pi))(1 - 1.25\sqrt{\sigma_a})$, $r = \sqrt{S/\pi}$, and $\sigma_a = S_a/S_s$ is the ratio of the chamber area S_a to the cross sectional area of the shared inlet volume S_s . The total impedance of chamber B can be found in a similar way. The smeared impedance of both lower chambers, at the boundary defined by points A and B, is given as

$$\zeta_{AB} = \frac{\zeta'_A \zeta'_B}{\zeta'_A \sigma_b + \zeta'_B \sigma_a} \quad (3)$$

The impedance translation theorem is then used to calculate the specific acoustic input impedance for the pair of resonators just below the facesheet as [9]

$$\zeta_i = \left(\frac{S_a + S_b}{S_s} \right) \left(\frac{\zeta_{AB} \cos(kh_s) + j\rho c \sin(kh_s)}{\cos(kh_s) + j\zeta_{AB} \sin(kh_s)/(\rho c)} \right) \quad (4)$$

where h_s is the depth of the shared inlet volume. The first term in parenthesis accounts for the small area change introduced by the strip of material just below the facesheet.

2. Facesheet Transfer Impedance

The transfer impedance of the facesheet is estimated using the two parameter model as [10]

$$\zeta_{\text{fs}} = \theta_{\text{lin}} + \theta_{\text{nonlin}} + \theta_{\text{gf}} + i\chi_{\text{fs}} \quad (5)$$

where θ_{lin} is the viscous contribution to the facesheet resistance, θ_{nonlin} is the nonlinear component of resistance, θ_{gf} is the grazing flow component of resistance, and χ_{fs} is the mass reactance of the facesheet. The viscous component of the facesheet resistance is defined as

$$\theta_{\text{lin}} = \frac{a\mu t}{2\rho c(\sigma_{\text{fs}}C_D)d^2} \quad (6)$$

where a is an empirical constant typically set to 64, μ is the dynamic viscosity of air, t is the facesheet thickness, ρ is the density of air, σ_{fs} is the open area ratio of the facesheet, C_D is the discharge coefficient typically defined as 0.771, and d is the facesheet hole diameter. The nonlinear resistance, θ_{nonlin} , is neglected in this study since a relatively low source sound pressure level of 120 dB is used for the evaluation. The grazing flow resistance is defined as

$$\theta_{\text{gf}} = \frac{M_{\text{CL}}}{\sigma_{\text{fs}}\{2 + 1.256(\delta^*/d)\}} \quad (7)$$

where M_{CL} is the freestream Mach number and δ^* is the boundary layer displacement thickness, which is assumed to equal 0.069" for the $M_{\text{CL}} = 0.3$ test condition [11]. The normalized mass reactance of the facesheet is

$$\chi_{\text{fs}} = \frac{k(t + \varepsilon d)}{\sigma_{\text{fs}}C_D} \quad (8)$$

where ε is the hole length end correction multiplier, defined as

$$\varepsilon = \frac{0.85(1 - 0.7\sqrt{\sigma_{\text{fs}}})}{1 + 305M_{\text{CL}}^3} \quad (9)$$

It is important to note that the two parameter model is a semiempirical model originally developed by industry to model representative facesheets with grazing flow. The model tends to be less accurate when there is no flow. Therefore, nonstandard empirical coefficients for a and C_D are used for those cases. Specifically, a is assumed to equal 320 and C_D is set to 1.16 as described in Ref. [12]. In contrast, the standard empirical coefficients are used to predict the transfer impedance of the facesheet with grazing flow.

3. Smeared Surface Impedance

The total impedance of each resonator, or pair of resonators, is found by adding the transfer impedance of the facesheet to the input impedance of the resonators, $\zeta'_i = \zeta_i + \zeta_{\text{fs}}$. While mass end corrections can be used to approximate the radiation loading in specific situations, no additional end corrections are used in this study since a more accurate finite element model is available to refine the design. Therefore, the smeared surface impedance is calculated as

$$\zeta_s = 1/\beta_{\text{avg}} \quad (10)$$

where β_{avg} is the spatially averaged admittance defined as

$$\beta_{\text{avg}} = \sum_{i=1}^{N_r} [\sigma_i/\zeta'_i] \quad (11)$$

where σ_i is the ratio of the inlet area to the total surface area of the sample, and N_r is the total number of resonators, or pairs of resonators in the case of Fig. 2(b), in the array.

B. Finite Element Model

While the semianalytical model is efficient, approximations are needed to model wave propagation within the samples, particularly at the interface between the lower chambers and the shared inlet volume. Additional corrections are also needed to capture the radiation loading on the resonators. Therefore, a more accurate, but also more computationally expensive, finite element model is used in conjunction with the semianalytical model to refine the design.

The finite element model, like the semianalytical model, is used to predict the smeared surface impedance of the acoustic liner samples. Specifically, a three dimensional model of an impedance tube is created with the liner sample positioned at one end of the tube. While the core is modeled explicitly, the effect of the facesheet is captured with the same two parameter transfer impedance model without grazing flow that was previously described. The impedance tube is excited with a plane wave source opposite the liner sample. Both the sample and tube are meshed using a hybrid grid containing both structured and unstructured components. The mesh uses quadratic Lagrange elements, with a maximum size at least 10 times smaller than the acoustic wavelength. Symmetry is leveraged to reduce the size of the models, which typically have less than 10k degrees of freedom. The acoustic response is found by solving the Helmholtz equation in the frequency domain from 500 Hz to 3000 Hz in 50 Hz increments. While solve times vary based on the liner sample, an average run time on a standard laptop (i7-6820HQ processor with 16 GB RAM) is 0.2 seconds per frequency. For comparison, solve times for the semianalytical model are 3 to 4 orders of magnitude faster. Finally, point predictions are processed using the transfer function method to calculate the specific acoustic impedance of the sample [13].

V. Liner Design

Prototype liners are designed to assess the tradeoffs between conventional variable depth liners and the new variable depth concept with shared inlet volumes. The general characteristics of the liner samples are described first, followed by the specific design details. The first two sets of samples are designed for the NASA Langley Normal Incidence Tube (NIT), which is an impedance tube with a 2" by 2" cross section. The samples, therefore, have an active area of 2" by 2", with 0.25" shoulders around the perimeter to facilitate mounting in the test apparatus. A cross sectional cut of the core is depicted in Fig. 3(a), where the solid material is shown in blue and the resonators are in white. The core contains sixteen 0.4" by 0.4" chambers arranged in a 4 by 4 array. As Fig. 3(a) shows, the samples are half symmetric, with the distribution of chamber depths indicated by labels D1-D8. In this case, the chamber depth refers to the distance from the facesheet to the rigid wall at the back of each chamber. The samples with shared inlet volumes include small, 0.3" deep volumes just below the facesheet that couple pairs of resonators, as depicted in Fig. 2(b). When present, the shared inlet volumes couple D1 to D5, D2 to D6, D3 to D7, and D4 to D8.

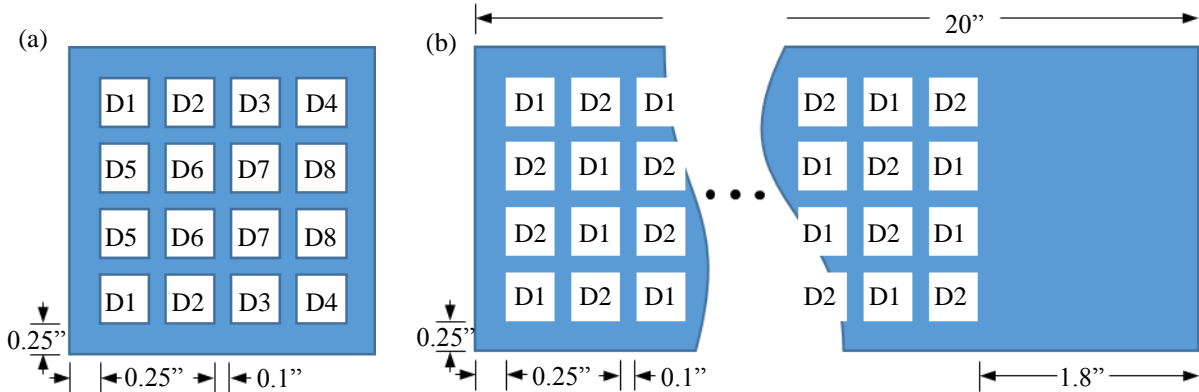


Fig. 3 Resonator layout in the (a) NIT sample and (b) GFIT sample.

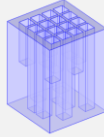
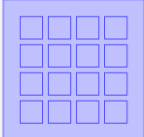
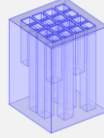
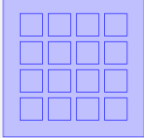
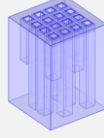
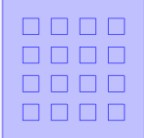
The final set of samples is designed for the NASA Langley Grazing Flow Impedance Tube (GFIT), which is a 2.5" tall by 2" wide flow duct used to measure the acoustic properties and relative drag of liner samples exposed to both sound and grazing flow. The cross sectional cut of the core of a GFIT liner sample is depicted in Fig. 3(b). Once again, the resonators have a square cross section with dimensions of 0.4" by 0.4", but in this case the core contains 144 chambers arranged in a 4 by 36 array. The samples include 0.25" shoulders around the perimeter and a 1.8" long solid section at the end to simplify mounting in the test apparatus. In this case, only two unique depths are used in the design, indicated by D1 and D2 in Fig. 3(b). Once again, when present, the shared inlet volumes are 0.3" deep and couple pairs of neighboring resonators.

A. Design 1: NIT Multitonal Design

The first set of samples are designed to highlight the fundamental differences between conventional variable depth liners and the new type of variable depth concept with shared inlet volumes. To simplify the comparison, perforated facesheets are not included and each sample only contains two unique chamber depths tuned for either 1000 or 2000 Hz. In other words, the samples are designed to have zero reactance at those frequencies. Approximate chamber

depths are determined first by setting Eqs. (1) and (4) equal to zero and then solving for h . The equations, however, neglect the radiation loading at the surface of the liner sample. Therefore, the finite element model is used to refine the design and select the final chamber depths. The final designs are given in Table 1. Since the samples are designed without perforated facesheets, a thin strip of material, as depicted in Fig. 2(b), was added on top of the shared inlet volume sample, SIV1a, to reduce the open area ratio and match the conventional variable depth sample, VD1. This was done to simplify the comparison between the two samples. A second shared inlet volume sample, SIV1b, was built with identical core geometry, but with smaller 0.283" by 0.283" openings in the top of the core. The top surfaces of all three samples are covered by a wire mesh, with a nominal resistance of 120 MKS Rayls.

Table 1 Description of the first set of NIT samples.

Sample label	Chamber depths, in	Core	Facesheet	Sample open area ratio	Top view
Variable Depth (VD1)	(D1, D2, ..., D8) = 1.63, 3.32, 1.63, 3.32, 3.32, 1.63, 3.32, 1.63		120 MKS Rayl wire mesh	0.64	
Shared Inlet Volume (SIV1a)	(D1, D2, ..., D8) = 1.74, 3.43, 1.74, 3.43, 3.43, 1.74, 3.43, 1.74		120 MKS Rayl wire mesh	0.64	
Shared Inlet Volume (SIV1b)	(D1, D2, ..., D8) = 1.74, 3.43, 1.74, 3.43, 3.43, 1.74, 3.43, 1.74		120 MKS Rayl wire mesh	0.32	

B. Design 2: NIT Broadband Design

The second set of samples are designed to highlight inherent tradeoffs associated with broadband designs. In this case, a perforated facesheet is included in the design and the samples have eight unique chamber depths. While the facesheet thickness and hole diameter are specified as 0.035" and 0.020", respectively, the open area ratio is a design variable along with the depth of the eight chambers. The overall goal of the design is to minimize the fraction of incident energy reflected from the surface of the sample from 1000 to 3000 Hz. Specifically, the objective function is calculated by equally weighting the arithmetic mean and maximum value of the reflected energy over the desired frequency range as

$$F = \langle R_i \rangle + \max_i(R_i) \quad (12)$$

where

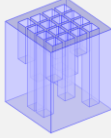
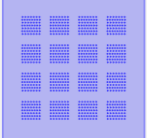
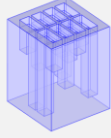
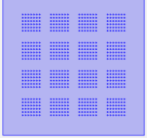
$$R_i = \left| \frac{\zeta_s(f_i) - 1}{\zeta_s(f_i) + 1} \right|^2 \quad (13)$$

is the fraction of incident energy reflected, $|\dots|$ denotes the complex modulus (i.e., absolute value), f_i is the selected frequency, $\langle \dots \rangle$ is the arithmetic mean over the set of frequencies, and \max_i is the maximum value of the set. For this study, the frequency vector extends from 1000 to 3000 Hz in 50 Hz increments. Note that the absorption coefficient is defined as $\alpha = 1 - R_i$. Therefore, minimizing Eq. (12) is equivalent to maximizing the absorption coefficient from 1000 to 3000 Hz.

The same design process is used for both the conventional variable depth sample and the shared inlet volume concept to see if similar acoustic performance can be achieved with less open area ratio. Specifically, the samples are designed in two steps. A genetic algorithm is used first to search for a global optimum. To reduce the size of the design

space, the local open area ratio of the facesheet is bounded between 0.01 and 0.5, and the chamber depths are bounded between 0.2" and 5.5". Constraints are also imposed to limit the search increments to 0.01 for the open area ratio and 0.04" for the chamber depths. In this case, the semianalytical impedance model is used to calculate the objective function since the genetic algorithm requires tens of thousands of function evaluations. The search is complete when the average relative change in the objective function, defined in Eq. (12), is less than 10^{-6} over 500 consecutive generations, with a population size of 90. While there is significant variability between runs, an average run converges in approximately 700 generations and requires 63k function evaluations. While the semianalytical model is computationally efficient, it uses approximations and is, therefore, not expected to identify the true global optimum. However, if the solution is close to optimal, then the more accurate, but also more computationally expensive, finite element model can be used to search for a local minimum near that solution. Specifically, this step is performed using a simplex search method developed by Ref. [14] and implemented within `fminsearch` [15]. Once again, there is variability between runs, but the solution tends to converge in several hundred function evaluations. The final designs are included in Table 2.

Table 2 Description of the NIT samples designed for broadband absorption.

Sample label	Chamber depths, in	Core	Facesheet (as built)	Sample open area ratio (as built)	Top view of facesheet
Variable Depth (VD2)	(D1, D2, ..., D8) = 1.40, 2.28, 0.77, 2.87, 2.97, 0.93, 1.79, 1.12		Perforate $t = 0.035''$ $d = 0.020''$ ($t = 0.034''$ $d = 0.022''$)	0.065 (0.079)	
Shared Inlet Volume (SIV2)	(D1, D2, ..., D8) = 1.19, 2.03, 0.88, 2.74, 3.18, 0.90, 1.41, 0.96		Perforate $t = 0.035''$ $d = 0.020''$ ($t = 0.032''$ $d = 0.023''$)	0.053 (0.070)	

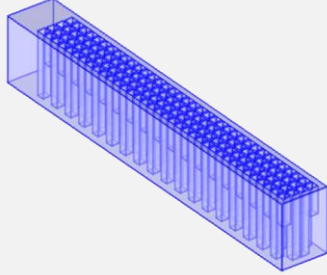
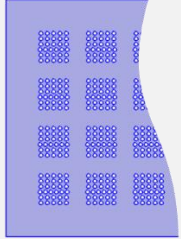
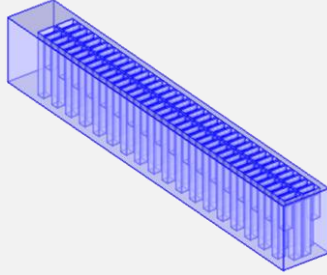

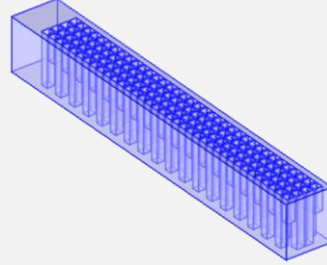

C. Design 3: GFIT Multitonal Design

The third set of samples are designed to assess differences in relative liner drag and acoustic performance in the GFIT. The resonator layout is depicted in Fig. 3(b). Once again, the samples include perforated facesheets with a specified thickness and hole diameter. The open area ratio is, however, a design variable along with the depth of two chambers. The goal of the design is to achieve a normalized smeared surface impedance of $\zeta_{\text{target}} = 1 + 0j$ at two discrete frequencies, 1000 and 2000 Hz. More specifically, the samples are designed to minimize the difference between the designed impedance ζ_s and the target impedance ζ_{target} , using the objective function,

$$F = \left(\sum_{i=1}^{N_f} W_i |\zeta_{\text{target}}(f_i) - \zeta_s(f_i)|^2 \right)^{0.5} \quad (14)$$

where N_f is the total number of frequencies in the set, and W_i is a weighting parameter equal to one when f_i is 1000 or 2000 Hz, otherwise $W_i = 0$. The samples are designed using the previously described two step approach. The final designs are shown in Table 3. The first two samples are designed to minimize the objective function in Eq. (14) using three design variables, whereas the facesheet open area ratio of the third sample is constrained during the design to match the open area ratio of SIV3. The purpose of this final design is to determine if similar reductions in the open area ratio of the conventional sample can be achieved without sacrificing acoustic performance.

Table 3 Description of the GFIT samples.

Sample label	Chamber depths, in	Core	Facesheet (as built)	Sample open area ratio (as built)	Top view of facesheet
Variable Depth (VD3a)	(D1, D2) = 1.413, 3.28		Perforate: $t = 0.035''$ $d = 0.040''$ ($t = 0.040''$) ($d = 0.038''$)	0.153 (0.141)	
Shared Inlet Volume (SIV3)	(D1, D2) = 1.516, 3.181		Perforate $t = 0.035''$ $d = 0.040''$ ($t = 0.040''$) ($d = 0.038''$)	0.074 (0.068)	
Variable Depth (VD3b)	(D1, D2) = 1.244, 2.717		Perforate $t = 0.035''$ $d = 0.040''$ ($t = 0.040''$) ($d = 0.038''$)	0.074 (0.068)	

VI. Experimental Setup

In addition to the three sets of samples previously described, an additional smooth wall sample was also fabricated to serve as the baseline for the relative drag calculations. All samples were 3D printed using a stereolithography process. Following fabrication, the samples were measured to ensure the as-built dimensions were consistent with the design. The measured dimensions, when different from the design, are included in Tables 1-3 in red.

A. Normal Incidence Tube (NIT)

The first two sets of liner samples were tested in the NASA Langley Normal Incidence Tube (NIT), depicted in Fig. 4. The normal incidence tube has a 2" by 2" interior cross section with acoustic drivers installed in the end of the tube opposite the liner sample. A reference microphone 0.25" from the surface of the sample is used to set the sound pressure level, and two additional microphones installed in a rotating plug are used to measure the sound pressure 2.5" and 3.75" from the surface of the sample. The two microphone technique, with microphone switching, is used to calculate the impedance of the sample based on the pressure measurements. The tests included in this study were

conducted using a time varying sine sweep source with a reference sound pressure level of 120 dB [16]. The frequency resolution of the processed data is approximately 5 Hz.

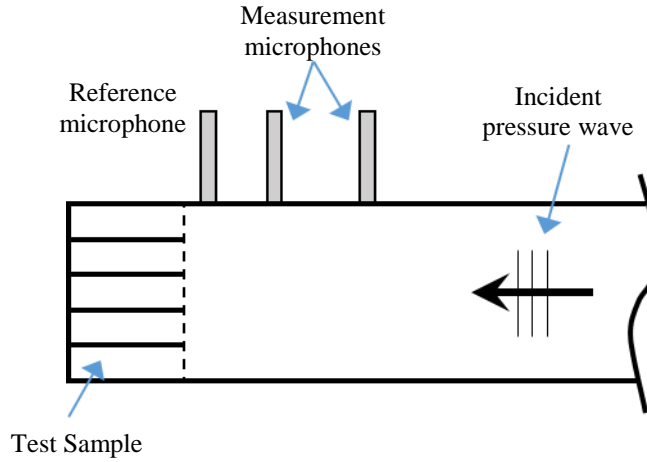


Fig. 4 Schematic of the NASA Langley Normal Incidence Tube (NIT).

B. Grazing Flow Impedance Tube (GFIT)

The third set of samples was tested in the NASA Langley Grazing Flow Impedance Tube (GFIT), which is a 2.5" tall by 2" wide waveguide used to measure the acoustic properties and relative drag of liner samples exposed to high sound pressure levels and grazing flow (i.e., flow parallel to the facesheet). The bottom and sides of the GFIT are rigid, while a portion of the top wall can be replaced with a sample liner, as depicted in Fig. 5. For this study, the leading edge of the GFIT samples were positioned 8" downstream from the source plane. The centerline Mach number was set to 0.3 and the source sound pressure level, generated using an upstream array of acoustic drivers, was set to 120 dB. The tests were performed at discrete frequencies from 400 to 3000 Hz in 200 Hz increments. Acoustic measurements were acquired using an array of flush mounted microphones embedded in the walls of the duct. Aft of the measurement section, the flow duct is terminated by a quasianechoic diffuser. The liner impedance is deduced using an implementation of the Prony method [17] described in Ref. [18]. This method performs well away from resonant and antiresonant frequencies [19]. A second reduction method, based on the convected Helmholtz equation, was therefore used to determine the impedance at resonance [20]. No attempt was made to update the values at antiresonance.

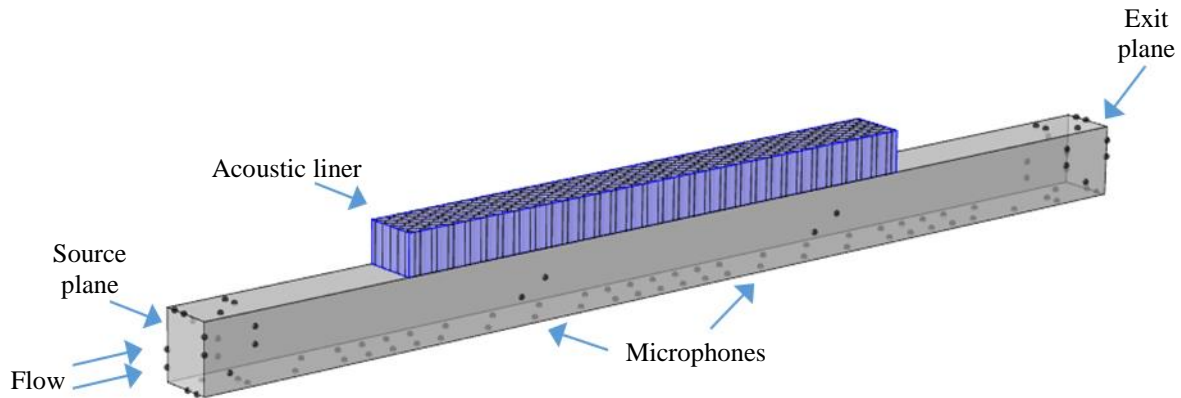


Fig. 5 Sketch of the NASA Langley Grazing Flow Impedance Tube (GFIT) measurement section.

Static pressure measurements were acquired at the same flow speed, but with the acoustic drivers off. While the acoustic component of liner drag can be important at high sound pressure levels (e.g., around 150 dB), the low levels used in this test were expected to have no appreciable impact on liner drag [3]. The liner resistance factor was calculated based on the static pressure drop measurements as described in Ref. [21].

VII. Results

Measurements, and in some cases predictions, are used to compare the proposed liner concept to a standard variable depth design. The comparison begins with normal incidence impedance measurements and concludes with in-duct attenuation and relative liner drag measured in the GFIT.

A. Normal Incidence (Designs 1 & 2)

The measured impedance spectra for the first set of NIT samples are shown in Fig. 6. As expected, the reactance, in Fig. 6(b), is approximately zero at 1000 and 2000 Hz for both the conventional variable depth sample, VD1, and the shared inlet volume sample, SIV1a. The resistance, on the other hand, varies from 0.5 for VD1 to 0.3 for SIV1a at the same frequencies. This occurs despite the fact that both samples have the same open area ratio and are covered with the same wire mesh. To understand why, it helps to think about the effective open area ratio, which is defined as the fraction of the top surface area of the sample that has a nonzero acoustic velocity. Both samples have an equal number of resonators targeting 1000 and 2000 Hz. In the standard variable depth sample, however, the response at each frequency is largely controlled by only half the resonators. Therefore, the effective open area ratio at the design frequencies is roughly half of the physical open area ratio. In contrast, the acoustic velocity at the surface of the shared inlet sample is much more uniform since one of the underlying resonators will be excited at each frequency. All of the inlets are therefore active at both 1000 and 2000 Hz, which means the effective open area ratio is approximately equal to the physical open area ratio. Since the smeared resistance is inversely proportional to the effective open area ratio, and the shared inlet sample has a larger effective open area ratio, the corresponding resistance is less.

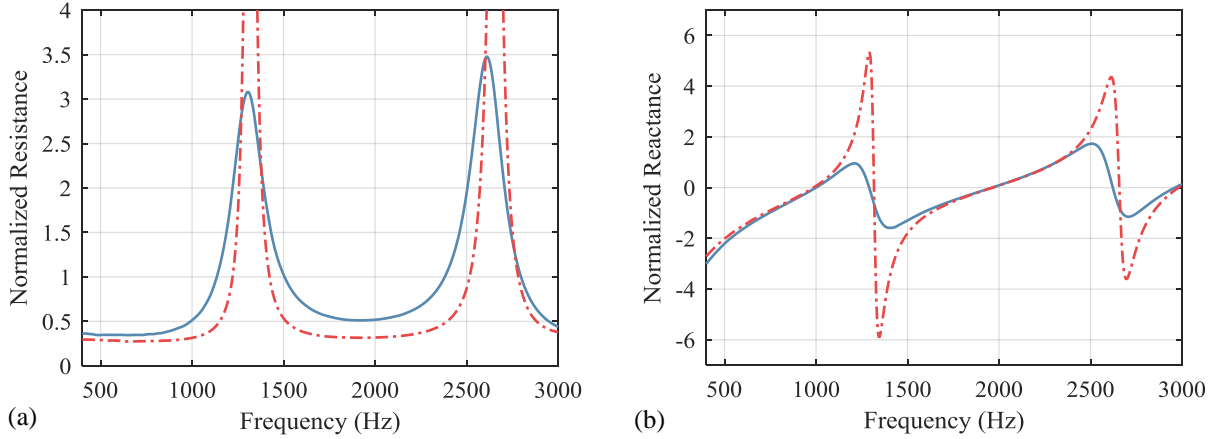


Fig. 6 Measured normalized impedance spectra for VD1 (—) and SIV1a (---).

The previous comparison demonstrated that the shared inlet volume design can be used to reduce the smeared resistance without changing the open area ratio. Therefore, it should be possible to reduce the overall open area ratio of the shared inlet sample while maintaining the same resistance as the original variable depth sample. This is confirmed in Fig. 7(a) and Fig. 7(b), which compares the measured impedance spectra for VD1 with the measured spectra for SIV1b. Recall that SIV1b includes an inlet area contraction that reduces the open area ratio by a factor of two relative to VD1. In this case, both samples have approximately the same resistance at resonance. The area contraction, however, introduces additional mass reactance that shifts the reactance to the left by a small amount. The resulting absorption spectra are compared in Fig. 7(c). Note that while there are differences, the peak levels are similar even though SIV1b has half the open area ratio. The shift in the peak absorption is, once again, due to the mass reactance introduced by the area contraction, and the differences in the peak amplitude are caused by small differences in resistance. While these differences could be eliminated by making small changes to the area contraction and chamber depths, the differences off resonance are unavoidable. Specifically, the absorption spectrum for SIV1b has a more pronounced dip around 1300 Hz. To understand why, recall that the surface of the standard variable depth sample is composed of a collection of inlets connected to independent resonators tuned for different frequencies. Therefore, the antiresonances (i.e., frequencies where the acoustic velocity is zero at the resonator inlets) will be different. In contrast, the acoustic velocity at the surface of the shared inlet sample is more uniform since all inlets are connected to identical pairs of resonators. Thus, the antiresonances are aligned, resulting in a more pronounced dip between the natural frequencies.

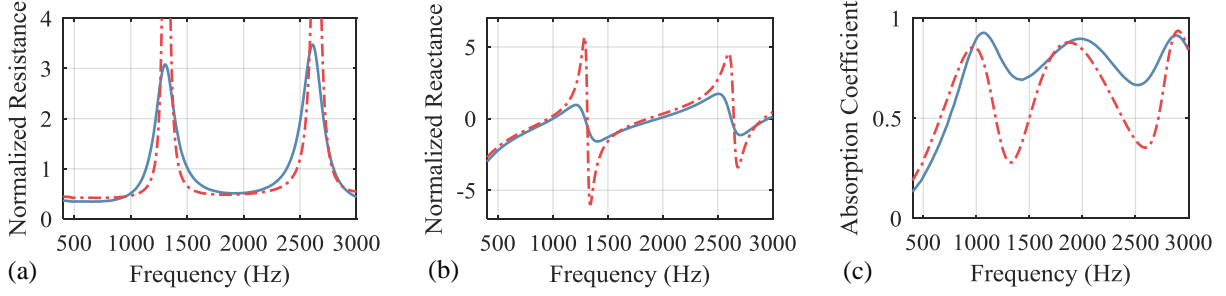


Fig. 7 Measured spectra for VD1 (—) and SIV1b (---) showing: (a) normalized resistance, (b) normalized reactance, and (c) absorption.

The previous comparison considered samples with two unique chamber depths. Additional chamber depths, however, could be added to smooth the response and improve the broadband performance. The second set of NIT samples have eight unique chamber depths designed to minimize the reflected energy (i.e., maximize the absorption) from 1000 to 3000 Hz. This set of samples also includes facesheets with different open area ratios. The measured normalized impedance spectra for the broadband samples are compared in Fig. 8. Note that reflected energy is minimized when the normalized resistance is one and the reactance is zero. As the spectra show, the measured impedance oscillates about the optimal values.

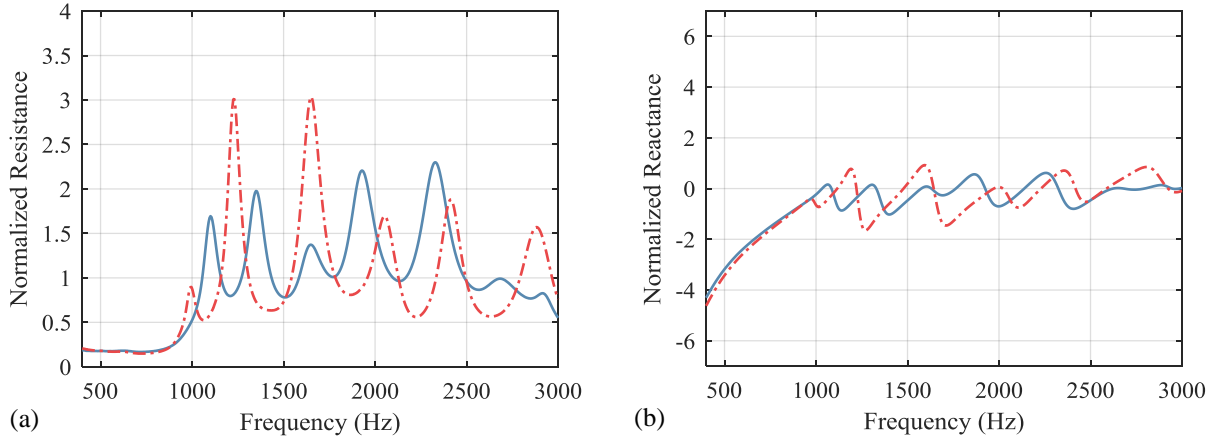


Fig. 8 Measured normalized impedance spectra for VD2 (—) and SIV2 (---).

The corresponding measured absorption coefficient spectra are shown in Fig. 9(a), along with design predictions in Fig. 9(b), and updated predictions using the as-built dimensions in Fig. 9(c). The favorable agreement between Fig. 9(a) and Fig. 9(c) confirms that the acoustic finite element model accurately predicts absorption. Therefore, it is reasonable to assume that the absorption would have been similar to Fig. 9(b) if the fabricated sample was closer to the original design. Nevertheless, it is clear that the standard variable depth sample has a smoother response than the sample with shared inlet volumes. This is, once again, due to differences in the way the antiresonances combine. Overall, the acoustic performance of the sample with shared inlet volumes is slightly worse than the standard design, but the shared inlet sample has 18% less open area. Therefore, it appears that tradeoffs between liner drag and acoustic performance are necessary when broadband attenuation is the goal.

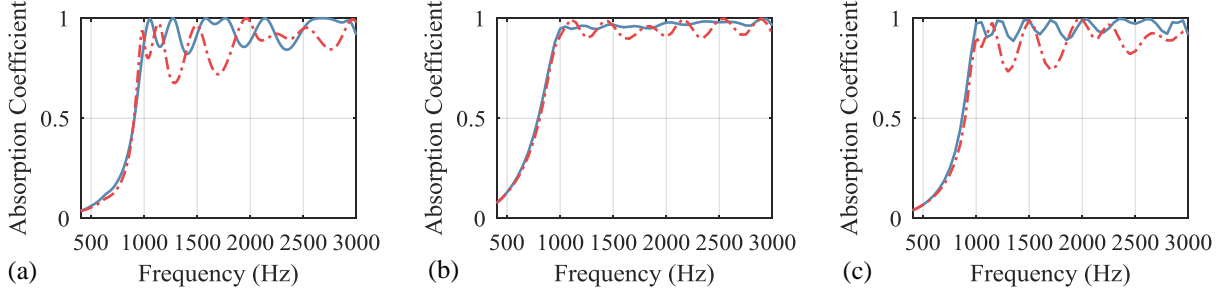


Fig. 9 Absorption spectra for VD2 (—) and SIV2 (---) showing: (a) measurements, (b) original design predictions, and (c) updated predictions using the as-built dimensions.

B. Grazing Flow (Design 3)

The third set of samples were designed to assess differences in acoustic performance and relative liner drag in the GFIT with grazing flow at Mach 0.3. For this comparison, a multitonal metric was selected, which is better suited for the shared inlet volume design. Specifically, the samples were designed to have a normalized resistance of one and reactance of zero at 1000 and 2000 Hz, as indicated by the yellow dots in Fig. 10(a) and Fig. 10(b). The educed impedance spectra for the samples is also plotted for comparison. While the educed reactance of both samples matches the target at the design frequencies, the resistance comparison is not as good. The educed resistance is noticeably less than the target. In this case, the offset is not due to geometric differences between the designed and as-built samples. Instead, the discrepancy is attributed to the grazing flow resistance term in the two parameter model. The underlying reason for this discrepancy will be investigated in a future study. Despite the apparent problem with the transfer impedance model, both samples have a nearly identical resistance of 0.5 at 1000 Hz. Since there is no spatial variation within the facesheet, and the samples have the same number of resonators tuned for 1000 and 2000 Hz, the resistance should be similar at both resonant frequencies. However, the educed resistance for VD3a at 2000 Hz is closer to 0.2, less than half the resistance of SIV3. This discrepancy is not yet understood. Nevertheless, the two samples perform similarly in terms of the measured in-duct attenuation, as shown in Fig. 10(c). In this case, in-duct attenuation refers to the change in the measured sound pressure level between the source and termination planes. Both samples provide 20-30 dB attenuation at the design frequencies. This confirms that the shared inlet volume design can provide similar tonal attenuation as the standard variable depth liner with half the open area ratio.

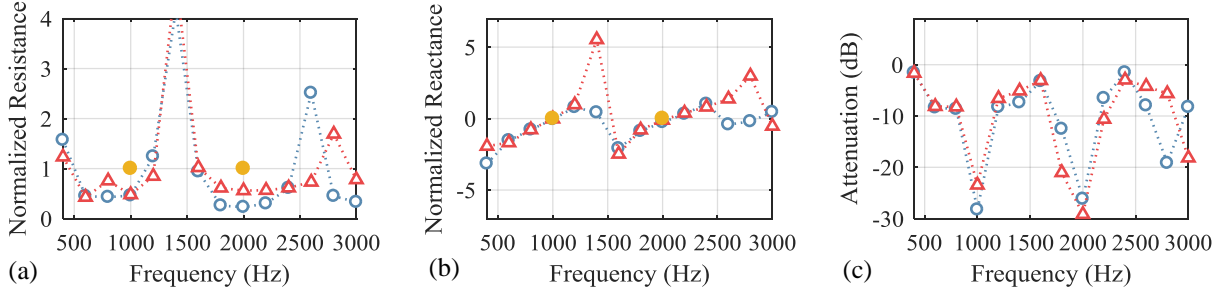


Fig. 10 Measured spectra for VD3a (---○---) and SIV3 (---△---) showing: (a) normalized resistance, (b) normalized reactance, and (c) in-duct attenuation. The target impedance is indicated by (●).

A second variable depth sample, VD3b, was also designed and tested to see if a conventional sample, constrained to the same open area ratio as SIV3, could match the impedance and achieve similar in-duct attenuation. The comparison of VD3b and SIV3 is shown in Fig. 11. As expected, VD3b has a higher resistance than the shared inlet volume sample at both 1000 and 2000 Hz. This, in turn, results in less in-duct attenuation at those frequencies, as shown in Fig. 11(c).

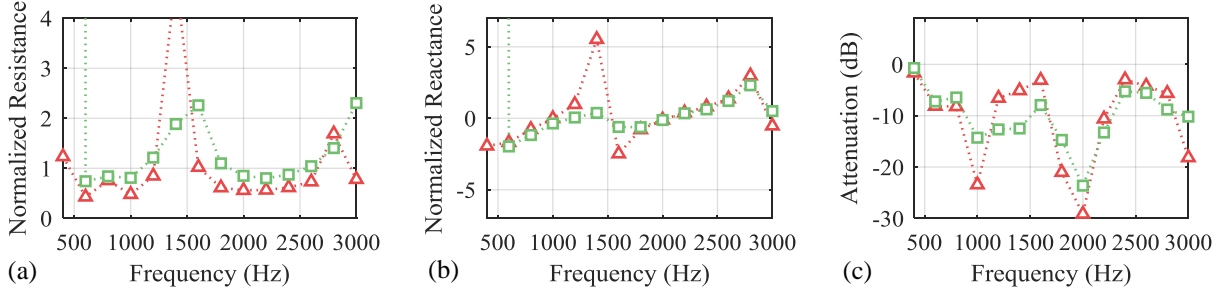


Fig. 11 Measured spectra for SIV3 (---△---) and VD3b (---□---) showing: (a) normalized resistance, (b) normalized reactance, and (c) in-duct attenuation.

Static pressure measurements were acquired during the tests to quantify the differences in relative liner drag. Specifically, liner resistance factors were calculated from five sets of static pressure measurements. The mean values are plotted in Fig. 12(a), along with error bars representing 95% confidence intervals. Results show that the liner resistance factor for SIV3 is significantly less than VD3a. In contrast, the differences between SIV3 and VD3b are not statistically significant, which was expected since those samples use identical facesheets. The relative liner drag, or drag penalty, can be calculated from the liner resistance factors as $\Delta\lambda_L = \lambda_L - \lambda_{SW}$, where λ_L is the liner resistance and λ_{SW} is the resistance of the smooth wall sample. The relative liner drag is compared in Fig. 12(b). The results show that the mean relative liner drag of SIV3 is 75% less than VD3a. Recall that this reduction in drag is achieved without sacrificing acoustic performance, as shown in Fig. 10(c). In contrast, the second variable depth sample, VD3b, provides a similar reduction in relative liner drag, but this change comes at the expense of some acoustic performance, as shown in Fig. 11(c).

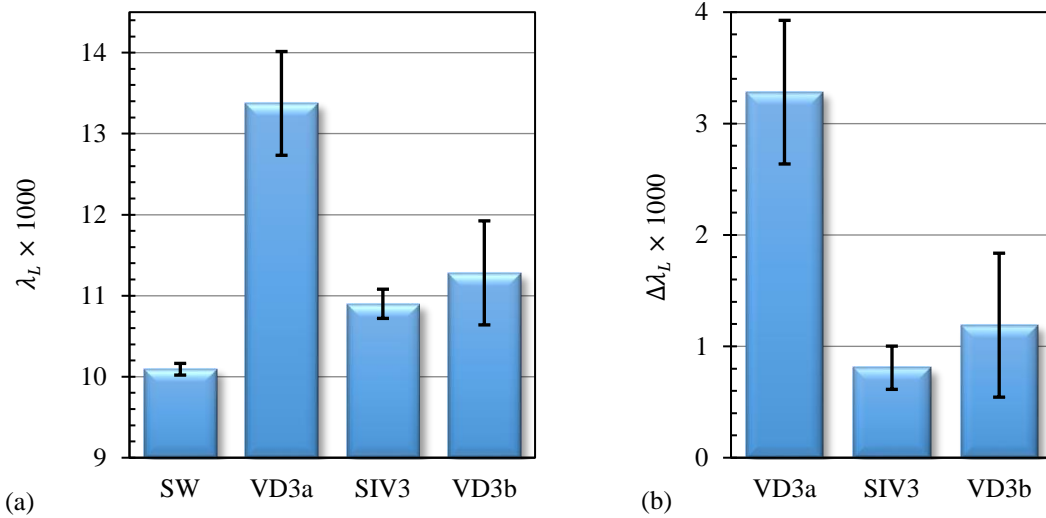


Fig. 12 Measurements of the (a) liner resistance factor and (b) relative liner drag with Mach 0.3 grazing flow and no sound.

The objective function selected for this final comparison was particularly well suited for the shared inlet volume design. As previously seen, the benefits can be less compelling when the objective function is broadband. Therefore, the shared inlet volume concept is not expected to outperform conventional variable depth liners in all applications, but could be beneficial when drag is critical and the objective function is dominated by a discrete set of frequencies.

VIII. Concluding Remarks

The purpose of this study was to evaluate a new type of variable depth acoustic liner, which has the potential to reduce the liner drag penalty relative to more conventional variable depth designs without sacrificing acoustic performance. Results, in terms of in-duct attenuation and relative liner drag, were presented for both types of liners. The main findings of the study are listed below:

- The shared inlet volume design can achieve the same impedance as a more conventional variable depth sample at discrete frequencies with 50% less open area ratio.
- The reactance spectrum for the shared inlet volume concept has more frequency variation than a comparable variable depth sample.
- Broadband samples designed to maximize the normal incidence absorption coefficient from 1000-3000 Hz were compared. In this case, the optimal shared inlet volume sample had 18% less open area than a comparable variable depth sample. The reduction in open area was accompanied, however, by a slight reduction in broadband acoustic performance.
- Measurements collected with Mach 0.3 grazing flow confirm that the shared inlet volume sample can reduce the relative liner drag by up to 75% while providing comparable in-duct attenuation as a conventional variable depth liner at discrete frequencies. Similar reductions in the relative liner drag could not be achieved with a conventional variable depth sample without sacrificing acoustic performance.

In summary, this study demonstrated that the shared inlet volume concept can reduce the liner drag penalty by up to 75% while providing similar tonal attenuation as a conventional variable depth sample. While the proposed design concept is well suited for multitonal objective functions, tradeoffs between liner drag and acoustic performance may be necessary if broadband attenuation is required. Therefore, the shared inlet volume concept is not always a replacement for conventional variable depth designs, but could be beneficial in certain applications, particularly when drag is critical and the objective function is dominated by discrete frequencies. Follow-on tests are planned to assess if the concept can be combined with low drag facesheets (e.g., facesheets with perpendicular slots) to further reduce the drag penalty without sacrificing acoustic performance.

Acknowledgments

The contributions of Robert Andrews and Alonzo ‘Max’ Reid are gratefully acknowledged for their role in sample preparation and testing. Funding for this activity was provided from the NASA Advanced Air Transport Technology Project under the Advanced Air Vehicles Program.

References

- [1] Howerton, B. M., and Jones, M. G., “Acoustic liner drag: measurements on novel facesheet perforate geometries,” AIAA Paper 2016-2979, *22nd AIAA/CEAS Aeroacoustics Conference*, June 2016.
- [2] Nark, D. M., and Jones, M. G., “Design of an advanced inlet liner for the Quiet Technology Demonstrator 3,” *25th AIAA/CEAS Aeroacoustics Conference*, May 2019. Submitted.
- [3] Howerton, B. M., and Jones, M. G., “A conventional liner acoustic/drag interaction benchmark database,” AIAA Paper 2017-4190, *23rd AIAA/CEAS Aeroacoustics Conference*, June 2017.
- [4] Parrott, T. L., and Jones, M. G., “Parallel-element liner impedances for improved absorption of broadband sound in ducts,” *Noise Control Engineering Journal*, Vol. 43, No. 6, 1995.
- [5] Jones, M. G., Nark, D. M., Watson, W. R., and Howerton, B. M., “Variable-depth liner evaluation using two NASA flow ducts,” AIAA Paper 2017-3022, *23rd AIAA/CEAS Aeroacoustics Conference*, June 2017.
- [6] Tijdeman, H., “On the propagation of sound waves in cylindrical tubes,” *Journal of Sound and Vibration*, Vol. 39, No. 1, 1975.
- [7] Ingard, U., “On the theory and design of acoustic resonators,” *Journal of the Acoustical Society of America*, Vol. 25, No. 6, 1953.
- [8] Schiller, N. H., and Jones, M. G., “Smeared impedance model for variable depth liners,” AIAA Paper 2018-3774, *24th AIAA/CEAS Aeroacoustics Conference*, June 2018.
- [9] Pierce, A. D., *Acoustics: an introduction to its physical principles and applications*, Acoustical Society of America, Melville, New York, 1989, pp. 139.
- [10] Jones, M. G., Parrott, T. L., and Watson, W. R., “Uncertainty and sensitivity analyses of a two-parameter impedance prediction model,” AIAA Paper 2008-2928, *14th AIAA/CEAS Aeroacoustics Conference*, May 2008.
- [11] Parrott, T. L., and Jones, M. G., “Chapter 6 – Uncertainty in acoustic liner impedance measurement and prediction,” *Assessment of NASA’s Aircraft Noise Prediction Capability*, edited by Milo D. Dayl, NASA/TP-2012-215653, July 2012, pp. 157-204.
- [12] Schiller, N. H., Jones, M. G., and Bertolucci, B., “Experimental evaluation of acoustic engine liner models developed with COMSOL Multiphysics,” AIAA Paper 2017-4186, *23rd AIAA/CEAS Aeroacoustics Conference*, June 2017.
- [13] ASTM E1050-12, *Standard test method for impedance and absorption of acoustical materials using a tube, two microphones and a digital frequency analysis system*, ASTM International, West Conshohocken, PA, 2012.
- [14] Lagarias, J. C., Reeds, J. A., Wright, M. H., and Wright P. E., “Convergence properties of the Nelder-Mead simplex method in low dimensions,” *SIAM Journal of Optimization*, Vol. 9, No. 1, 1998, pp. 112–147.
- [15] The Mathworks, Inc., Natick, Massachusetts, *MATLAB Optimization Toolbox*, version 9.2.0.556344 (R2017a), 2017.

- [16] Howerton, B. M., Vold, H., and Jones, M. G., “Application of swept sine excitation for acoustic impedance eduction,” *25th AIAA/CEAS Aeroacoustics Conference*, May 2019. Submitted.
- [17] Marple, S. L., *Digital spectral analysis with applications*, Prentice–Hall, Upper Saddle River, NJ, 1987, pp. 203–250.
- [18] Jones, M. G., Watson, W. R., Howerton, B. M., and Busse-Gerstengarbe, S., “Effects of mean flow assumption and harmonic distortion on impedance eduction methods,” *AIAA Journal*, Vol. 53, No. 6, 2015.
- [19] Watson, W. R., Carpenter, M. H., and Jones, M. G., “Performance of Kumaresan and Tufts algorithm in liner impedance eduction with flow,” *AIAA Journal*, Vol. 53, No. 4, 2015.
- [20] Watson, W. R., and Jones, M. G., “Impedance eduction in ducts with higher-order modes and flow,” AIAA Paper 2009-3236, *15th AIAA/CEAS Aeroacoustics Conference*, May 2009.
- [21] Howerton, B. M., Jones, M. G., and Jasinski, C. M., “Acoustic liner drag: further measurements on novel facesheet perforate geometries,” AIAA Paper 2018-3605, *24th AIAA/CEAS Aeroacoustics Conference*, June 2018.